Check for updates

ADVANCED THEORY AND SIMULATIONS
www.advtheorysimul.com

Effect of Atomic Charges on $C_2H_2/CO_2/CH_4$ Separation Performances of Covalent-Organic Framework Adsorbents

Hakan Demir and Ilknur Erucar**

A critical factor for the accuracy of computational screening studies is the method employed to assign atomic charges. While chemically meaningful atomic charges can be obtained using a quantum chemistry method-based charge assignment technique (density-derived electrostatic and chemical method (DDEC6)), its application to large material datasets remains computationally demanding. As an alternative, machine-learning (ML) models can offer the ability to determine atomic charges with high accuracy and speed. Herein, two ML models, Partial Atomic Charge Predicter for Porous Materials based on Graph Convolutional Neural Network (PACMAN) and Partial Atomic Charges in Metal-Organic Frameworks (PACMOF), are utilized to predict atomic charges in Clean, Uniform, Refined with Automatic Tracking from Experimental Database (CURATED) covalent-organic frameworks (COFs). The predicted atomic charges are used in simulations to assess COFs' $C_2H_2/CO_2/CH_4$ separation performances in comparison with reference DDEC6-based performances. Results show PACMAN charges can more effectively reproduce DDEC6-based charges and corresponding separation performance metrics, underscoring their suitability for high-throughput material screening. Additionally, the proportions of Coulombic interactions to van der Waals interactions are systematically analyzed, revealing substantial variation across both narrow and wide pores. This study highlights that ML models can be applied to obtain atomic charges that could enable attaining accurate material performance evaluations.

1. Introduction

Acquiring pure acetylene (C_2H_2) is vital for industrial processes, as it can be utilized to produce several essential chemicals such as acetaldehyde, acetic acid, vinyl chloride etc. and used for metal processing.[1] Typically, C_2H_2 is produced via the partial combustion of methane (CH_4) or hydrocarbon cracking, leading to a gas mixture that includes CH_4 and carbon dioxide (CO_2) along with C_2H_2.[2,3] Separating C_2H_2 from this mixture, especially from CO_2, is challenging due to their similar boiling points and molecular sizes.[4] This separation is traditionally carried out via low-temperature distillation which is an energy-intensive process.[3] Alternatively, adsorption-based gas separation processes can provide energy-efficient operation at room temperature.[3] Achieving high gas separation performance, however, depends not only on the process design but also on selecting suitable adsorbent materials.

Covalent-organic frameworks (COFs) are a class of crystalline materials made up of light elements such as C, O, H, and B that are covalently linked to each other.[5,6] COFs can have high pore sizes and large surface areas as well as very low densities which can be beneficial for gas adsorption/separation applications.[7] As there can be a sheer number of building unit combinations that enable generating different COFs, experimental synthesis, characterization, and testing of each possible COF would be burdensome.[5,8,9] Due to time and cost constraints, experimental adsorption studies on COFs generally focus on a small list of structures. For instance, Wang et al.[10] synthesized imide-linked 2D COFs with different layer stackings and estimated their C_2H_2/CO_2 (1/1) separation performances using Ideal Adsorbed Solution Theory (IAST).[11] At ambient conditions, Nankai covalent organic frameworks ((NKCOF-11-AA) and NKCOF-11-ABC) were estimated to have C_2H_2/CO_2 selectivities of 2.6 and 3.2, respectively. Wang et al.[12] reported the synthesis of a quinoline-linked COF (COF-Q-CF_3) which was investigated for C_2H_2 and CH_4 adsorption/separation. At ambient conditions, it was determined that single-component C_2H_2 uptake in COF-Q-CF_3 was about six times as large as CO_2 uptake. Under the same conditions, C_2H_2/CH_4 (50/50) IAST selectivity of COF-Q-CF_3 was estimated to be 10. Chen et al.[13] investigated C_2H_2/CH_4 (50/50) and C_2H_2/CO_2 (50/50) separation in experimental samples of 2D sql COF and 3D pts COF. In 2D sql COF (3D pts COF), C_2H_2/CH_4 and C_2H_2/CO_2 IAST selectivities at ambient conditions were determined as 306.2 and 4.8 (8.4 and 3.8), respectively, where larger selectivity in 2D sql

H. Demir, I. Erucar
Faculty of Engineering, Department of Natural and Mathematical Sciences
Ozyegin University
Istanbul 34794, Turkey
E-mail: hakan.demir@atilim.edu.tr; ilknur.erucar@ozyegin.edu.tr
H. Demir
Department of Chemical Engineering
Atilim University
Incek, Ankara 06836, Turkey

The ORCID identification number(s) for the author(s) of this article can be found under https://doi.org/10.1002/adts.202500060

© 2025 The Author(s). Advanced Theory and Simulations published by Wiley-VCH GmbH. This is an open access article under the terms of the Creative Commons Attribution License, which permits use, distribution and reproduction in any medium, provided the original work is properly cited.

DOI: 10.1002/adts.202500060

COF was ascribed to higher accessibility of aldehyde groups. To the best of our knowledge, there is not any large-scale computational screening study investigating $C_2H_2/CO_2/CH_4$ separation in COFs in the literature. Here, some of the studies investigating the separation of binary gas mixtures involving C_2H_2 are summarized. In a joint experimental-theoretical study, Jiang et al.[14] measured single-component isotherms in Py-Na COF (involving 4,4′,4′′,4′′′-(pyrene-1,3,6,8-tetrayl) tetraaniline (PyTTA) and 2,5-di(oxypropane-1-sodium sulfonate) terephthalaldehyde (DSTA) unit with imine linkage) and estimated C_2H_2/CO_2 (50/50) IAST selectivity at room temperature to be larger than 7 between 0–1 bar. Their Grand Canonical Monte Carlo (GCMC) simulation results demonstrated that C_2H_2 uptake could be about twice the CO_2 uptake at ambient conditions. Through GCMC simulations and radial distribution function (RDF) analysis, Liu et al.[15] showed that in a fluorine-functioned COF (TpPa-F), C_2H_2 interacted with F atoms at closer distances than CO_2 which played a crucial role in having stronger C_2H_2 interaction with the framework.

One of the biggest advantages of GCMC simulations over experiments is the ability to acquire adsorption/separation performances of a large number of materials in a reasonable time enabling the investigation of not only a few structures but many. In recent years, a great number of studies employing atomistic simulations for gas adsorption/separation have been published where the number of COFs can vary in the order of hundreds to thousands.[16–20] Considering another kind of porous materials, metal-organic frameworks (MOFs), investigation of gas adsorption/separation performances of similar or even higher numbers of materials via GCMC simulations can be seen in the literature.[21–23] It has been shown earlier that partial atomic charges can have drastic effects on the adsorption/separation properties of porous materials.[21,24–30] For instance, Altintas et al.[21] studied CO_2/CH_4 adsorption (10/90 and 50/50) at room temperature in 1,500 MOFs using charge equilibration (Qeq)[31] and density-derived electrostatic and chemical (DDEC)[32] charges. Comparing CO_2 and CH_4 uptakes, CO_2/CH_4 adsorption selectivities, CO_2 working capacities, and CO_2 regenerabilities obtained using Qeq and DDEC charges, it was demonstrated that drastic differences could be seen for some MOFs. Lin et al.[24] calculated CO_2 Henry coefficients of MOFs using DDEC,[32,33] extended charge equilibration(EQeq),[34] and multilayer connectivity-based atom contribution (m-CBAC) charges where the Henry coefficients based on DDEC charges were used as reference data since the DDEC method relies on quantum chemistry (i.e., density functional theory (DFT)) calculations. It was determined that the correlation between Henry coefficients obtained using m-CBAC charges and DDEC charges was stronger than that between Henry coefficients acquired via EQeq and DDEC charges. It was shown by Burner et al.[25] that CO_2 and H_2S uptakes based on MOF-electrostatic potential optimized Qeq charges (MEPO-Qeq)[35] could be drastically different than REPEAT[36] charges, especially at low pressures. Ongari et al.[28] employed different charge assignment methods (e.g., Qeq variants) and revealed that CO_2 volumetric uptakes at 298 K and 0.2 bar could be highly different than the reference (DDEC charge-based) uptakes highlighting the sensitivity of the results with respect to atomic charges. In a similar work, considering CO_2 uptakes calculated using different charge assignment methods in a specific MOF at 273 K, it was shown that significant differences could be seen across uptakes calculated using DDEC, QEq, and EQeq charges.[27] Similar conclusions were drawn in other works as well[26,29,30] stressing the crucial effect of partial charges on adsorption properties.

Recently, it has been shown that high-fidelity machine learning (ML) models can be constructed which can be used for the prediction of partial atomic charges and gas adsorption properties. With regard to the partial atomic charge prediction, Korolev et al.[37] developed an ML model where the DDEC6 charges of thousands of MOFs were used as reference data and showed that the model can reproduce DDEC6 charges very closely (mean absolute deviation $< 0.01\ e$). To test the transferability, the developed ML model was then used to predict charges of Clean, Uniform, Refined with Automatic Tracking from Experimental Database COFs (CURATED COFs)[9] where it was demonstrated that the mean absolute deviation (0.05 *e*) between DDEC6 charges and predicted charges was larger than that for MOFs which was ascribed to different local environments in MOFs and COFs. Luo et al.[26] constructed an ML model using REPEAT charges of more than 200,000 MOFs and demonstrated that the model could predict atomic charges with a mean absolute deviation of 0.025 *e*. Very recently, Pham et al.[38] developed ML models to assign partial atomic charges in neutral and ionic porous materials based on DDEC6 charges of ≈42,000 and 7,600 MOFs, respectively.

Regarding ML models to predict gas adsorption in COFs, De Vos et al.[18] demonstrated that by training ML models on single-adsorption data of ≈15,000 COFs (a selected diverse subset of more than 250,000 COFs) CO_2/N_2 (15/85) separation performances of COFs can be screened more efficiently than brute-force methods as accurate ML predictions pave the way for identifying top performers rapidly. Similarly, Aksu et al.[17] developed ML models using adsorption data of more than 7,000 COFs to predict CO_2/CH_4 (50/50) separation performances of large number of unseen COFs (about one order of magnitude larger). In a separate work by Aksu et al.,[39] using simulated gas uptakes in more than 1,000 COFs, a number of ML models were developed which were subsequently used to obtain gas uptakes (and thus, separation performances) of ≈70,000 COFs in seconds. As the separations investigated were of several kinds (CO_2/CH_4, CO_2/H_2, CO_2/N_2, CH_4/H_2, CH_4/N_2, and O_2/N_2), this study showed the wide applicability of combining simulations and ML techniques. Lang et al.[40] studied He separation (He/CH_4 and He/N_2) using ≈1,000 synthesized MOFs via simulations and ML methods where it was shown that simulation-based He uptakes, He/CH_4, and He/N_2 adsorption selectivities could accurately be reproduced via ML models. Qiu et al.[41] showed that it is possible to identify top-performing COFs among tens of thousands of COFs for CH_4/H_2 (1/10) separation using high-throughput simulations and ML methods in conjunction. These foregoing studies showed that simulation-based results can be reproduced accurately using ML models as long as proper selection of data, featurization, and models is performed.

In this work, the role of partial atomic charges on the $C_2H_2/CO_2/CH_4$ (0.33/0.33/0.33) separation performances of ≈700 CURATED COFs[9] at 298 K is investigated where DDEC6, Partial Atomic Charge Predicter for Porous Materials based on Graph Convolutional Neural Network (PACMAN),[42]

© 2025 The Author(s). Advanced Theory and Simulations published by Wiley-VCH GmbH

25130390, 0, Downloaded from https://advanced.onlinelibrary.wiley.com/doi/10.1002/adts.202500060 by Ozyegin University, Wiley Online Library on [04/09/2025]. See the Terms and Conditions (https://onlinelibrary.wiley.com/terms-and-conditions) on Wiley Online Library for rules of use; OA articles are governed by the applicable Creative Commons License

and Partial Atomic Charges in Metal-Organic Frameworks (PACMOF)[29] ML model-based charges are utilized in GCMC simulations. PACMOF model, a random forest model, was developed using ≈320,000 partial atomic charges involved in ≈3,000 MOFs obtained from the Computation-Ready Experimental Metal–Organic Framework (CoRE MOF) 2019 database.[43] In comparison, PACMAN model is a graph convolution neural network model constructed using more than 1.8 million partial atomic charges of ≈17,000 Quantum MOFs (QMOFs).[44] Considering the element-wise distribution of partial atomic charges, the number of partial atomic charges assigned for a particular element could be two orders of magnitude higher in PACMAN model compared to PACMOF model which can serve as an advantage for getting more accurate charges in PACMAN model. While larger data sets could be useful for getting high-fidelity predictions, it should be noted that other factors (diversity of dataset, sampling method) also play vital roles in affecting model accuracy.[45] Both ML models can provide rapid partial atomic charge predictions (in seconds for structures with small unit cells) while obtaining charges from ab-initio methods would typically take several orders of magnitude longer time which would be computationally infeasible for a large number of structures.

In this work, first, the distribution of partial atomic charges per element type is presented to highlight the discrepancies across different partial atomic charge assignment methods. Two sets of GCMC simulations are carried out to mimic vacuum swing adsorption (VSA) conditions (adsorption at 1 bar and desorption at 0.1 bar). Gas uptakes obtained via GCMC simulations are used to calculate separation performance metrics (adsorption selectivity, working capacity, and regenerability), which are then combined to rank COFs. The effects of partial atomic charges on gas uptakes, separation performances, and preferential gas siting are discussed. Besides, the breakdown of differences in partial atomic charges into atom types is presented. Finally, the effects of flexibility on the adsorption selectivity and contributions of Coulombic and van der Waals (vdW) interactions are demonstrated.

2. Computational Methods

CURATED COF database is a periodically updated database where addition/removal of certain structures can be observed across different versions. In this work, CURATED COF (July 2022 version) is employed which is originally comprised of 801 geometry-optimized structures with DDEC6[32,46–49] charges. The recently introduced ML models for atomic charge assignments named PACMAN and PACMOF are employed to acquire two other sets of atomic charges of CURATED COFs. PACMOF model was derived using DDEC6 and Charge Model 5 (CM5)[50] charges of a subset of CoRE-MOFs (2019 version)[43] as reference data while PACMAN model involves multiple models where charges of QMOFs[44] obtained using different methods (DDEC6, Bader,[51,52] CM5, REPEAT[36]) were employed as reference data. Herein, PACMOF and PACMAN ML model-based charges are obtained via the ML models based on DDEC6 charges as reference data. Note that in the coming sections, PACMOF and PACMAN ML model-based charges will be referred to as PACMOF and PACMAN charges in short.

All GCMC simulations to investigate $C_2H_2/CO_2/CH_4$ (0.33/0.33/0.33) separation at 298 K are performed using RASPA.[53] Models representing adsorbates are obtained from the literature.[54–57] To represent VSA conditions, two sets of GCMC simulations are carried out for each structure, one at adsorption pressure (1 bar) and the other at desorption pressure (0.1 bar). Equal initialization and production cycles are employed totaling 60,000 cycles where insertion/deletion, translation, rotation (except for CH_4), and molecule identity change moves are allowed which have equal probabilities. DREIDING[58] (Universal Force Field (UFF)[59]) force field parameters are used for atom types in COFs that are present (absent) in DREIDING force field to calculate Lennard-Jones interactions up to 12 Å. Lorentz–Berthelot mixing rules are employed to acquire cross-interaction terms. Electrostatic interactions are computed using Ewald summation.[60] The pore characteristics of COFs are determined using Zeo++[61,62] with a probe diameter of 3.68 Å, where applicable.

COFs having smaller pore-limiting diameters (PLDs) than the kinetic diameter of the largest adsorbate CH_4 (3.758 Å) are omitted together with COFs having no accessible surface area. Previously, it was noted that despite having a molecular size larger than the window size of rigid ZIF-8, N_2 could be adsorbed in ZIF-8.[63,64] This implies that there could be COFs that could adsorb all three adsorbates due to intrinsic and adsorbate-induced flexibility effects despite not satisfying PLD criterion. Considering this fact, while a smaller PLD value could have been chosen as a filtering criterion, the current PLD criterion was selected to discard COFs where adsorbates could potentially experience significant diffusion constraints. COFs in which adsorbate loadings deviate more than 15% around the mean value are discarded. Employing these filtering criteria resulted in 742 common COFs for which GCMC simulations using DDEC6, PACMAN, and PACMOF charges could be successfully completed.

The gas separation performances of COFs are evaluated based on three adsorbent separation performance metrics (i.e., adsorption selectivity, working capacity, and regenerability) which all rely on GCMC simulation results. The adsorption selectivity can be defined as $S_{ads,1/2} = \frac{N_1/N_2}{y_1/y_2}$ where N and y denote gas uptake in COFs and mole fraction of the gas species in the bulk mixture, successively. Working capacity is the difference between gas uptakes at adsorption and desorption conditions which can be mathematically shown as $\Delta N_1 = N_{ads,1} - N_{des,1}$ for gas species 1. Percent regenerability of a gas species (e.g., gas species 1) is defined as $R_1 = \frac{\Delta N_1}{N_{ads,1}} \times 100$. The COF rankings are determined by summing three individual separation performance scores ($Score_{X,i} = \frac{X_i}{X_{max}} \times 100$) where i designates material i. In this expression, $X_i(X_{max})$ represents the adsorption selectivity, working capacity or regenerability value of COF i (the maximum relevant metric value across all COFs). COFs with the highest total scores are assigned the highest rankings.

To investigate intrinsic flexibility effects using flexible snapshot method,[65] molecular dynamics (MD) simulations with a time step of 1.0 fs under NVT ensemble are carried out at 298 K using foregoing charge types and force field parameters for a production period of 5 ns using Large-scale Atomic/Molecular Massively Parallel Simulator (LAMMPS).[66,67] The cutoff distance is 12 Å as in GCMC simulations. Temperature control is established

© 2025 The Author(s). Advanced Theory and Simulations published by Wiley-VCH GmbH

25130390, 0, Downloaded from https://advanced.onlinelibrary.wiley.com/doi/10.1002/adts.202500060 by Ozyegin University, Wiley Online Library on [04/09/2025]. See the Terms and Conditions (https://onlinelibrary.wiley.com/terms-and-conditions) on Wiley Online Library for rules of use; OA articles are governed by the applicable Creative Commons License

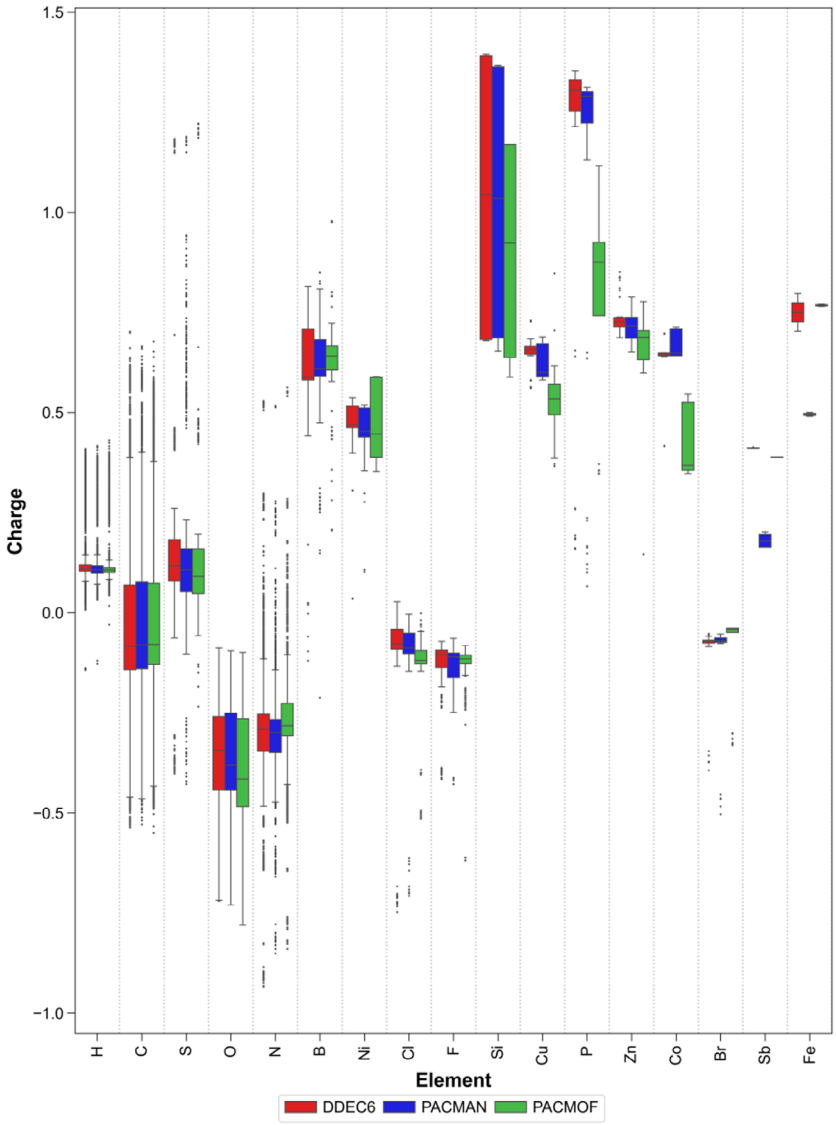

Figure 1. Distributions of partial atomic charges in CURATED COFs where distributions are categorized by charge assignment methods and element types.

using Nosé–Hoover thermostat with a 0.1 ps decay period.[68] Input files are generated using lammps-interface.[69] Five structure snapshots with equal time spacing (1 ns) are obtained from the MD trajectories. These snapshots (having no adsorbates) are employed in GCMC simulations as rigid CURATED COFs are used. GCMC simulation results are averaged over snapshots.

3. Results and Discussion

This investigation starts with the determination of partial atomic charges in COFs, as the simulation results rely on them. Separation performance metrics, including adsorption selectivity, working capacity, and regenerability, are then presented, calculated using gas uptakes obtained via GCMC simulations. Having determined top COFs using separation performance metrics, disparities across adsorption isotherms, RDFs, and partial charges in one of the top COFs (obtained using DDEC6, PACMAN, and PACMOF charges) are discussed. Finally, adsorption performances of COF snapshots and ratios of vdW and Coulombic interactions in rigid COFs are discussed together with those ratios in selected rigid and MD snapshots of COFs to demonstrate effect of intrinsic flexibility on interaction contributions.

3.1. Partial Atomic Charge Distributions

Figure 1 demonstrates DDEC6, PACMAN, and PACMOF charge distributions per element type in CURATED COFs. In general, DDEC6 and PACMAN charge distributions are similar albeit having some apparent exceptions like charges assigned to Fe, Sb, Co, and Cu atoms. In comparison, the dissimilarities between DDEC6 and PACMOF charge distributions are much

© 2025 The Author(s). Advanced Theory and Simulations published by Wiley-VCH GmbH

25130390, 0, Downloaded from https://advanced.onlinelibrary.wiley.com/doi/10.1002/adts.202500060 by Ozyegin University, Wiley Online Library on [04/09/2025]. See the Terms and Conditions (https://onlinelibrary.wiley.com/terms-and-conditions) on Wiley Online Library for rules of use; OA articles are governed by the applicable Creative Commons License

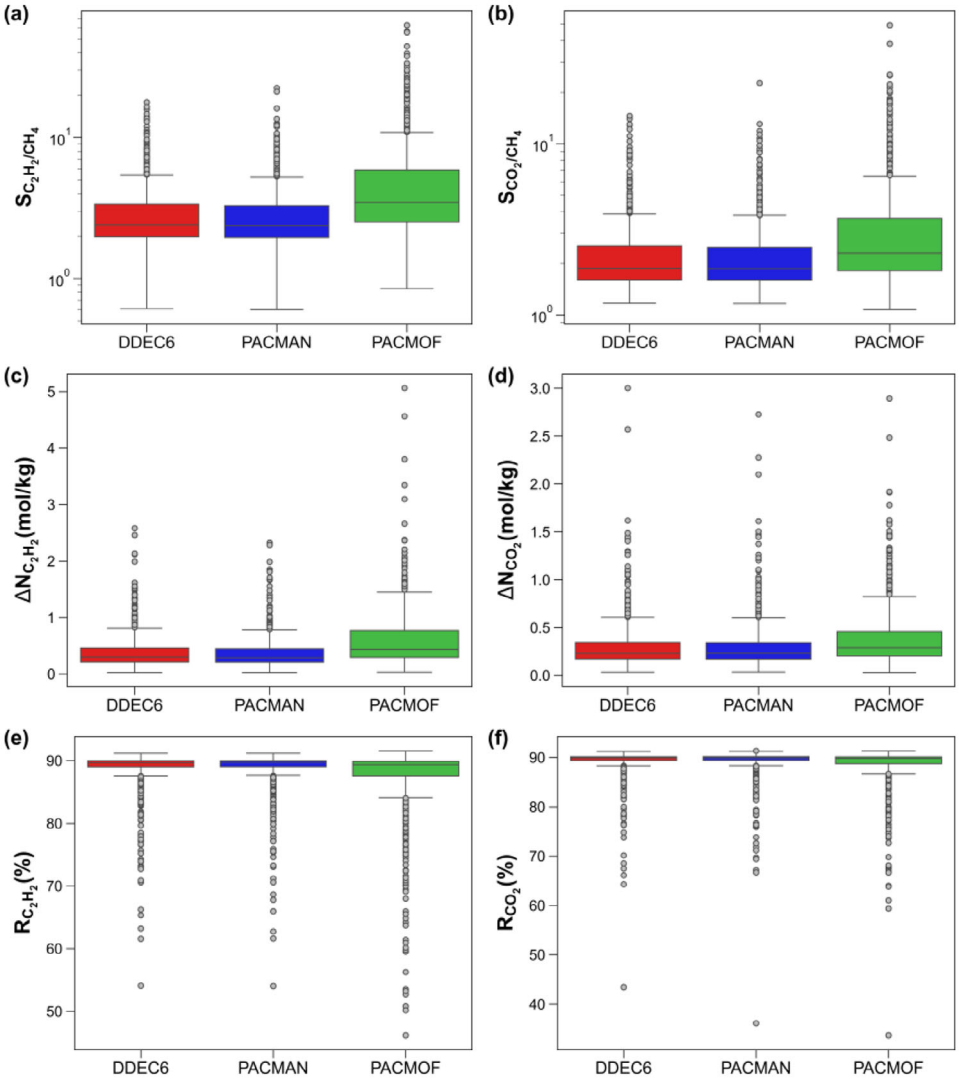

Figure 2. $C_2H_2/CO_2/CH_4$ separation performance metrics of CURATED COFs at 298 K as determined using DDEC6, PACMAN, and PACMOF charges. (The boxes demonstrate the values covered between the first and third quartiles (interquartile range). The whiskers indicate the top and bottom limits of the other values except for the outliers. Outliers, depicted as gray circles, are more than 1.5 quartiles away from either end of the boxes).

more pronounced as exemplified by charges of Cu, P, Co, B, Ni, Cl, Si, Fe, and Br atoms. Given MOFs and COFs are different classes of materials, the local atomic environment properties in MOFs can be different than those in COFs (e.g., bond distance, coordination number, average electronegativity of coordination shells). As the local atomic environment properties are features of the ML models used, these potentially different inputs of COFs that were not used during ML model development can lead to disparities across DDEC6 charges and the ML-predicted charges. Therefore, the transferability of the ML models can be achieved/improved if local atomic environments that are similar to those in COFs are used/added in ML model training. It has been shown earlier that an improved description of local atomic environments around atoms can result in higher fidelity predictions.[29] Recently, it has been noted that PACMOF model was trained on a relatively small training set of MOFs (≈3,000 MOFs) with limited sampling of chemical diversity and it may not provide charges at DDEC6 quality for underrepresented structures.[38]

3.2. $C_2H_2/CO_2/CH_4$ Separation Performance Metrics

Figure 2 displays the spreads of $C_2H_2/CO_2/CH_4$ separation metrics (namely adsorption selectivity, working capacity, and regenerability) of CURATED COFs where C_2H_2 and CO_2 are considered as desired species (for removal) over the undesired species CH_4. These separation metrics are calculated for three different cases where the structures are assigned DDEC6, PACMAN, and PACMOF charges. In panel (a), C_2H_2/CH_4 adsorption selectivities of CURATED COFs are plotted where they span the ranges of 0.61–17.78, 0.60–22.48, and 0.85–62.65 based on DDEC6, PACMAN, and PACMOF charges, respectively. Within these ranges, the majority of the C_2H_2/CH_4 adsorption selectivities lie in the

© 2025 The Author(s). Advanced Theory and Simulations published by Wiley-VCH GmbH

25130390, 0, Downloaded from https://advanced.onlinelibrary.wiley.com/doi/10.1002/adts.202500060 by Ozyegin University, Wiley Online Library on [04/09/2025]. See the Terms and Conditions (https://onlinelibrary.wiley.com/terms-and-conditions) on Wiley Online Library for rules of use; OA articles are governed by the applicable Creative Commons License

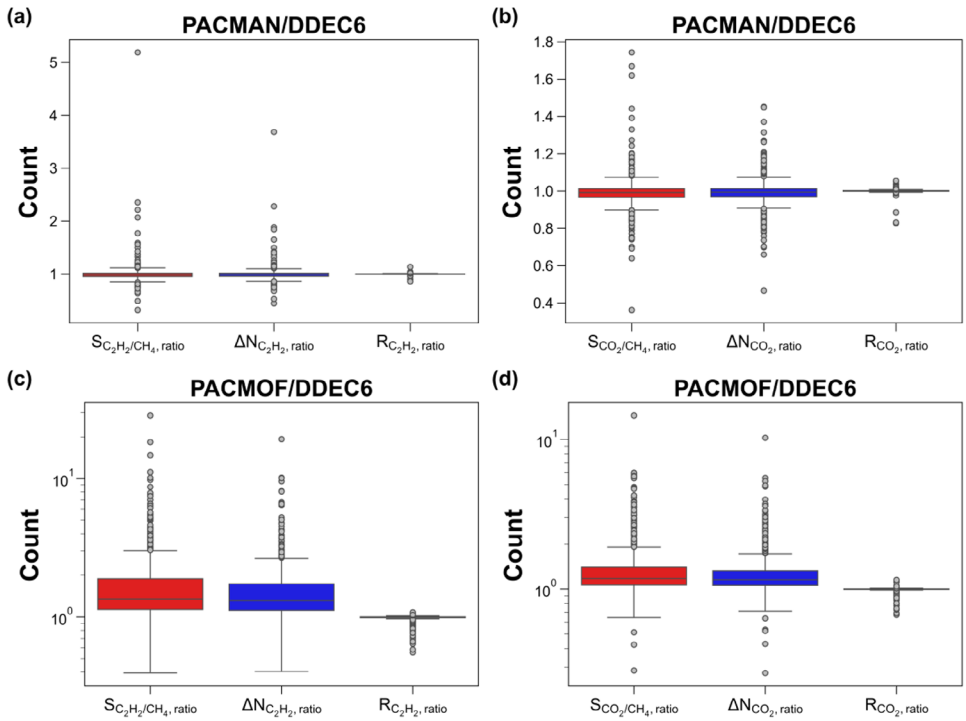

Figure 3. Distributions of the ratios of adsorption selectivity, working capacity, and regenerability. a,b) demonstrate the ratios of values obtained using PACMAN charges over those obtained using DDEC6 charges. c,d) show the ratios of values obtained using PACMOF charges over those obtained using DDEC6 charges.

range of 2–5. Panel (b) is the counterpart of panel (a) where CO_2/CH_4 adsorption selectivities are depicted. In general, these selectivities are lower than C_2H_2/CH_4 selectivities which can be ascribed to weaker CO_2 adsorption compared to C_2H_2. CO_2/CH_4 adsorption selectivities are in the ranges of 1.17–14.57, 1.16–22.65, and 1.07–49.34, respectively, according to GCMC simulation results employing DDEC6, PACMAN, and PACMOF charges. In panels (a, b), the largest C_2H_2/CH_4 and CO_2/CH_4 adsorption selectivities are acquired using PACMOF charges. Panel (c) demonstrates that the interquartile ranges of ΔN_{C2H2} based on DDEC6, and PACMAN charges (≈0.03–2.58 and ≈0.03–2.32 mol kg^{-1}) are much narrower than that of PACMOF charges (≈0.03–5.06 mol kg^{-1}). This suggests that many CURATED COFs perform similarly in terms of ΔN_{C2H2} based on DDEC6 and PACMAN charges. A similar conclusion can be drawn from panel (d) where the interquartile ranges of ΔN_{CO2} based on DDEC6, and PACMAN charges (0.17–0.35 and 0.17–0.34 mol kg^{-1}) are narrow and similar while that based on PACMOF charges shows a wider distribution (0.20–0.46 mol kg^{-1}). As demonstrated in panels (e, f), R_{C2H2} and R_{CO2} show similar distributions across different charge assignment/prediction methods although PACMOF distributions show some disparities compared to other two distributions towards the lower end.

It has been shown through Figure 2 that there can be different distributions of separation performance metrics according to the partial atomic charges used. **Figure 3** shows the ratios of separation performance metrics for each structure obtained using different charge assignment/prediction methods, specifically PACMAN/DDEC6 and PACMOF/DDEC6. Panel (a) suggests that for most of the CURATED COFs, using PACMAN charges, all three C_2H_2 separation performance metrics obtained (C_2H_2/CH_4 adsorption selectivity, C_2H_2 working capacity, C_2H_2 regenerability) are comparable with those acquired using DDEC6 charges (ratios close to 1). Panel (b) exhibits that the ratios of CO_2 separation performance metrics (PACMAN/DDEC6 based) are also around 1 for most of the CURATED COFs. Given these findings for the separation of interest, it can be deduced that using PACMAN charges in GCMC simulations can provide very similar adsorption selectivity, working capacity, and regenerability values to those obtained using DDEC6 charges. Panels (c,d) are analogous to panels (a,b) where the ratios of C_2H_2 and CO_2 separation performances metrics are obtained using PACMOF and DDEC6 charges. Looking at panels (c,d), the interquartile ranges are very narrow for both C_2H_2 and CO_2 regenerability while they are somewhat wider for adsorption selectivities and working capacities. While the ratios are mostly around 1–2, the outliers imply that there can be a factor of 10 or more in PACMOF/DDEC6 separation performance ratios. All in all, compared to PACMAN charges, PACMOF charges cause bigger disparities in the separation performance metrics with respect to DDEC6 charges.

As one of the ultimate goals of screening studies is identifying top performing materials, now we move on to the determination of top 20 CURATED COFs based on DDEC6, PACMAN, and PACMOF charges. Summing up three separation performance metrics for both C_2H_2 and CO_2, total separation performance scores are obtained, and rankings are determined where the top-ranked COF has the highest total separation performance score. Based on DDEC6 charges, the top 20 CURATED

© 2025 The Author(s). Advanced Theory and Simulations published by Wiley-VCH GmbH

25130390, 0, Downloaded from https://advanced.onlinelibrary.wiley.com/doi/10.1002/adts.202500060 by Ozyegin University, Wiley Online Library on [04/09/2025]. See the Terms and Conditions (https://onlinelibrary.wiley.com/terms-and-conditions) on Wiley Online Library for rules of use; OA articles are governed by the applicable Creative Commons License

COFs exhibit C_2H_2/CH_4 adsorption selectivities of 3.83–17.78, CO_2/CH_4 adsorption selectivities of 2.81–14.57, C_2H_2 working capacities of 0.68–2.58 mol kg^{-1}, CO_2 working capacities of 0.32–3.00 mol kg^{-1} as well as C_2H_2 and CO_2 regenerabilities above 70% (see Table S1, Supporting Information). As listed in Table S2 (Supporting Information), these top CURATED COFs typically have moderately or highly porous domains with PLDs (surface areas) reaching 18.73 Å (4,425.0 m^2 g^{-1}). The top 20 CURATED COFs based on PACMAN charges can show somewhat higher performances such as C_2H_2/CH_4 (CO_2/CH_4) adsorption selectivities reaching 22.48 (22.65) with similar pore characteristics (see Tables S3,S4, Supporting Information). Considering Table S5 (Supporting Information), the separation performance metrics of the top 20 CURATED COFs based on PACMOF charges are noticeably different than those of the top 20 COFs based on DDEC6 charges. Given the pore characteristics of these top CURATED COFs (Table S6, Supporting Information), there are cases where pore geometric property values (e.g., PLD, pore volume) can be drastically larger than those identified based on DDEC6 or PACMAN charges. Note that 14 of the top 20 CURATED COFs based on PACMAN charges are common with the top 20 structures based on DDEC6 charges. Considering that only 5 common CURATED COFs exist in the top 20 lists based on PACMOF and DDEC6 charges, PACMAN charges allow for a closer reproduction of DDEC6 charge-based rankings.

To understand the relative importances of separation performance metrics, the contributions of C_2H_2 and CO_2 separation performance metrics to the species-wise summed separation performance scores of the CURATED COFs are plotted in Figure S1 (Supporting Information). Based on DDEC6 and PACMAN charges, working capacities and regenerabilities contribute more than adsorption selectivities for the top 10 CURATED COFs while for the rest of the COFs, regenerabilities bear some more weight. In comparison, according to PACMOF charge-based results, regenerabilities contribute more than the other two metrics for most of the CURATED COFs. Having looked into relative contributions of separation performance metrics, now we examine the individual separation performance metrics of the top 10 CURATED COFs identified which are normalized by the maximum individual separation performance metrics among the top 10 materials. In panels (a, b) of Figure S2 (Supporting Information), most of the top 10 CURATED COFs based on DDEC6 charges perform well in terms of R_{CO2}, ΔN_{C2H2}, R_{C2H2} while some of them also excel at ΔN_{CO2}, C_2H_2/CH_4 and/or CO_2/CH_4 adsorption selectivity. Similar conclusions can be made regarding the top 10 CURATED COFs based on PACMAN charges. Yet, considering the top 10 CURATED COF performances based on PACMOF charges, it can be understood that among the first 5 CURATED COFs, there are materials which show strong performance in terms of all three C_2H_2 separation performance metrics. On the other hand, the top 6–10 CURATED COFs have relatively low $S_{C2H2/CH4}$, ΔN_{C2H2} and ΔN_{CO2} while excelling at R_{C2H2}. Note that the identified top COFs rely on the assumption of rigid framework in the simulations. It has been shown earlier that the flexibility effects on adsorption becomes pronounced in the cases where sizes of adsorbates and pores are similar.[70] As there are a few COFs with comparable PLDs to adsorbate sizes among top 20 COFs (based on all three charge types), the effect of flexibility on the calculated separation performance metrics can be expected to be significant while it would diminish for the other COFs with larger PLDs. This suggests that there could be differences between material rankings based on simulations employing rigid and fully flexible models.

3.3. $C_2H_2/CO_2/CH_4$ Adsorption Isotherms

Figure 4 demonstrates the C_2H_2, CO_2, and CH_4 adsorption isotherms for the top ranked CURATED COF (based on PACMOF charges) along with C_2H_2, CO_2, and CH_4 density plots using DDEC6 charges. Panel (a) shows the adsorption isotherms as determined using all three charge types where, as the pressure increases, PACMOF charge-based isotherms become drastically different than those obtained using PACMAN and DDEC6 charges. The differences in adsorption isotherms are apparent for C_2H_2 and CO_2 at all pressures, while they become clear for CH_4 after 1 bar. As PACMOF charges lead to much higher C_2H_2 and CO_2 loadings, and lower CH_4 loadings compared to those obtained using PACMAN and DDEC6 charges, 12011N2 appears as the top-ranking CURATED COF based on PACMOF charges, which does not exist in the top 20 CURATED COF lists based on PACMAN and DDEC6 charges. Since the adsorption isotherms obtained using PACMAN and DDEC6 charges are almost identical, it can be deduced for 12011N2 that using PACMAN charges enables reproducing all loadings obtained using DDEC6 charges. Note that the drastic differences in gas uptakes result in having 12011N2 as the top ranked material according to PACMOF charges, while it ranks 574th and 566th based on PACMAN and DDEC6 charges. In general, the agreements/disagreements between the loadings acquired using DDEC6 and other sets of charges considered here are material dependent and for other materials, different levels of agreement/disagreement may be seen. Panels (b, c, d) exhibit that while preferential adsorption sites (around pore walls) are similar for all sorbates, CO_2 and CH_4 molecules can also be found away from pore walls (towards pore center) which can be ascribed to strong C_2H_2 adsorption near pore walls displacing other sorbates. Figure S3 (Supporting Information) shows the RDFs of the gases in 12011N2 at 0.1 and 1 bar, 298 K where all three gas species prefer sites near H and O atoms based on DDEC6, PACMAN, and PACMOF charges. While RDFs based on DDEC6 and PACMAN charges are very similar, in comparison, those based on PACMOF charges imply that the probability of locating C_2H_2 and CO_2 molecules near O atoms of structures is relatively higher at close distances (3–4 Å).

Note that the employed DDEC6 charges are based on high-quality DFT calculations that can provide chemically meaningful charges. Their use in GCMC simulations can lead to close agreements between the simulated and experimental gas uptakes. Considering the single-component CO_2 isotherms in two CURATED COFs in **Figure 5**a,b, it can be deduced that the DDEC6-based isotherms can reproduce experimental isotherms closely. For these two materials, the PACMAN-based isotherms are also in close agreement with experimental isotherms. However, the agreement between the simulated and experimental uptakes is material dependent and lesser degree of agreement can be seen for different materials as shown for two different CURATED COFs in Figure 5c,d. Comparing DDEC6 and PACMAN-based isotherms, they are almost identical for 07010N3 and 07011N3,

© 2025 The Author(s). Advanced Theory and Simulations published by Wiley-VCH GmbH

25130390, 0, Downloaded from https://advanced.onlinelibrary.wiley.com/doi/10.1002/adts.202500060 by Ozyegin University, Wiley Online Library on [04/09/2025]. See the Terms and Conditions (https://onlinelibrary.wiley.com/terms-and-conditions) on Wiley Online Library for rules of use; OA articles are governed by the applicable Creative Commons License

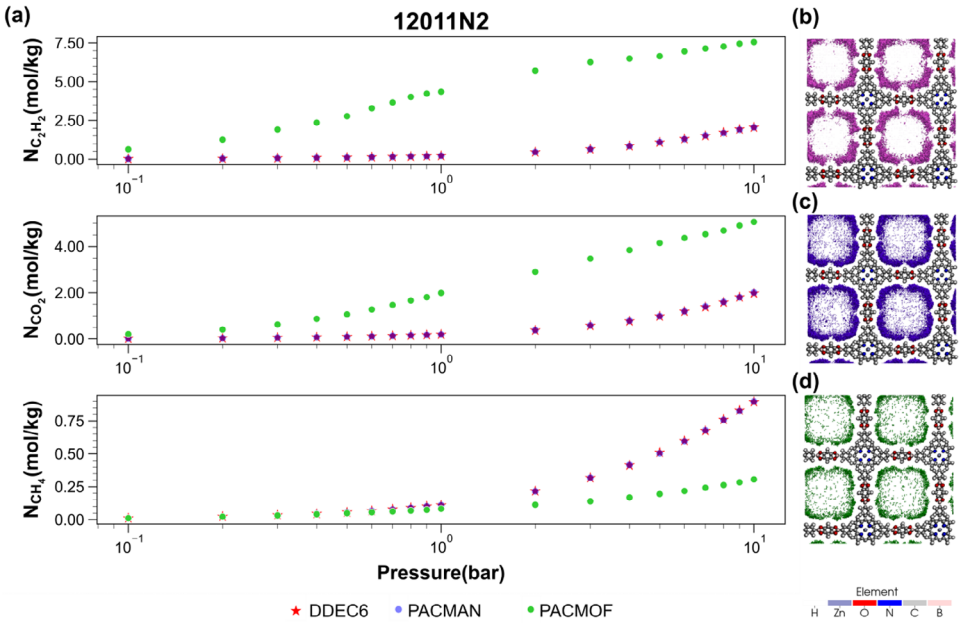

Figure 4. a) Adsorption isotherms of C_2H_2, CO_2, and CH_4 in 12011N2. Density plots of b) C_2H_2, c) CO_2, and d) CH_4 in 12011N2 (with DDEC6 charges).

while PACMOF-based isotherms deviate the most from experimental values and DDEC6-based uptakes. The discrepancies between experimental and simulated gas uptakes can be due to several different reasons. Firstly, although the structures used in this study are curated structures, they may not exactly represent the samples in experimental conditions. For instance, it has been highlighted earlier that low long-range crystallinity of COFs can lead to problems of resolving the structure.[9] Besides, as X-ray data does not provide adequate information on H atom positions, some discrepancies in the structures can be seen depending on the protocol followed to specify H atom positions.[9] As the atomic positions govern the gas-framework interactions, the differences

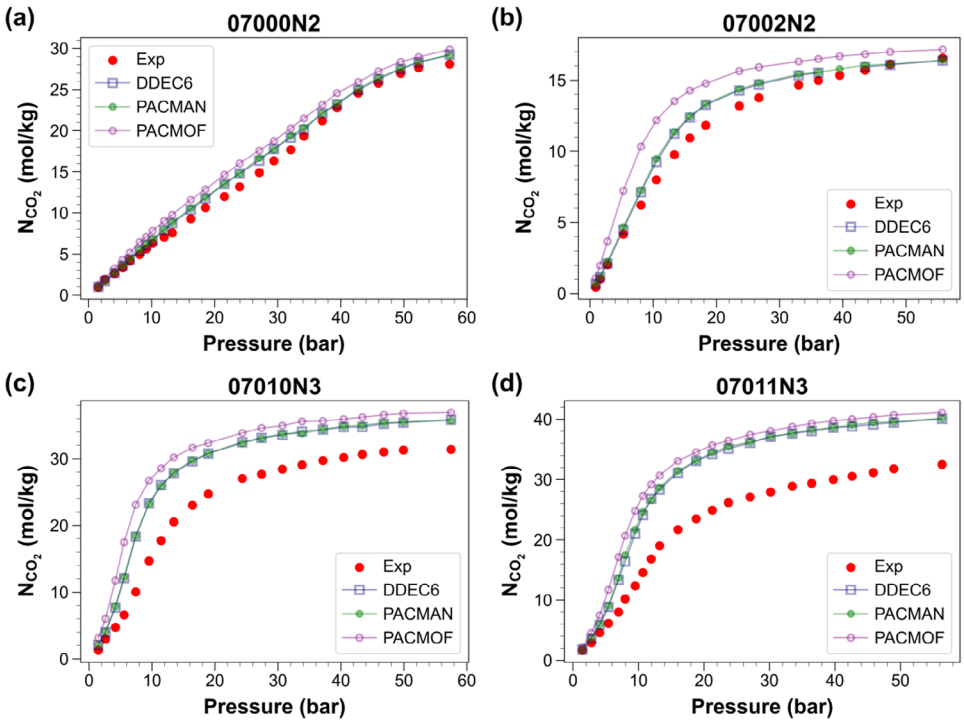

Figure 5. Comparison of experimental and simulated CO_2 uptakes in CURATED COFs at 298 K.

© 2025 The Author(s). Advanced Theory and Simulations published by Wiley-VCH GmbH

25130390, 0, Downloaded from https://advanced.onlinelibrary.wiley.com/doi/10.1002/adts.202500060 by Ozyegin University, Wiley Online Library on [04/09/2025]. See the Terms and Conditions (https://onlinelibrary.wiley.com/terms-and-conditions) on Wiley Online Library for rules of use; OA articles are governed by the applicable Creative Commons License

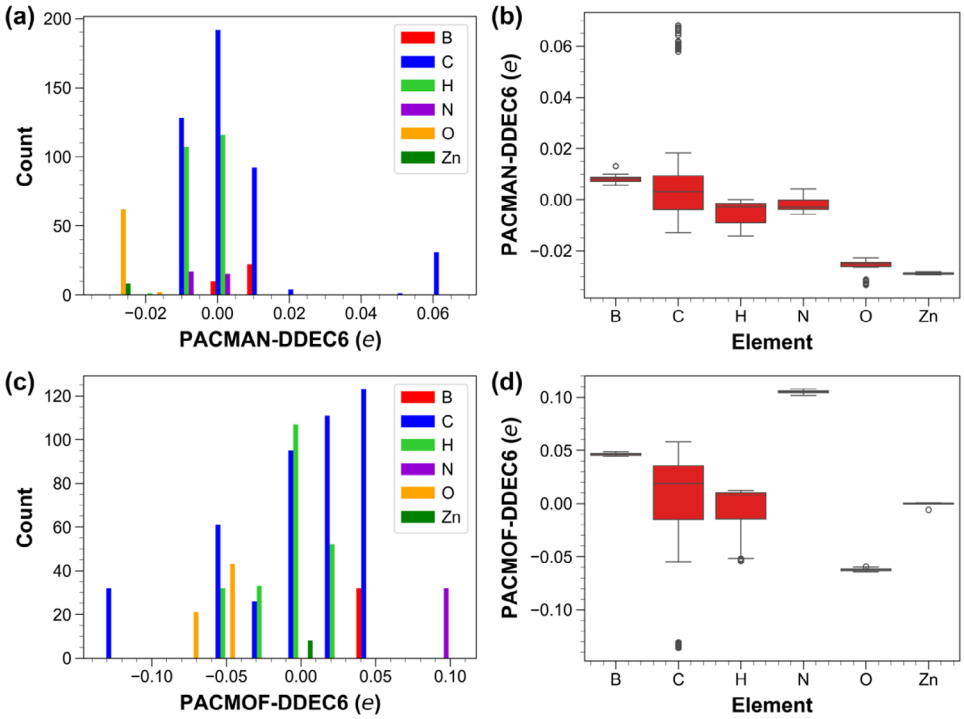

Figure 6. Distributions of partial atomic charge differences (a,b) PACMAN-DDEC6, and c,d) PACMOF-DDEC6) in 12011N2 per element type.

between experimental samples and simulation models can result in discrepancies in gas uptakes. In addition to uncertainties in determining experimental structures precisely, another important factor to consider with regard to agreement between experimental and simulated gas uptakes is structure flexibility. Higher uptakes observed in simulations can be ascribed to incomplete activation and/or imperfections of the experimental sample.[9]

3.4. Comparison of Partial Charges as Calculated Using Different Methods

Figure 6 displays the partial atomic charge differences in 12011N2 categorized by element types for PACMAN and PACMOF charges where DDEC6 charges are used as reference charges. Panel (a) shows a histogram of charge differences between PACMAN and DDEC6 where for more than 300 atoms (mainly C atoms) the charge differences are negligible. However, there are atoms where charge differences are somewhat larger than zero (in magnitude) such as some O atoms (< -0.02 *e*) and some C atoms (> 0.06 *e*). Panel (b) displays a boxplot form of these charge differences broken into element types. It shows that the most negative charge differences are obtained for Zn and O atoms (< -0.02 *e*). Most of the charge differences for C, B, H, and N atoms are near zero. Panel (c) demonstrates that while the charge differences (PACMOF-DDEC6) for a large number of atoms (mostly C, and H atoms) are almost zero, there is also a considerable number of atoms for which the charge differences are non-zero such as C atoms with a difference ≈0.05 *e*. Looking at panel (d), it can be understood that PACMOF-DDEC6 charge differences are almost zero for metal atoms (Zn) while there can be decent charge differences for non-metal atoms such as N, and C atoms (up to a magnitude of ≈0.10–0.15 *e*).

3.5. Effect of Flexibility on Interactions and Gas Separation Performances

Figure 7 shows the relative contributions of Coulombic and vdW interactions between host and gas species in CURATED COFs calculated using DDEC6, PACMAN, and PACMOF charges. Specifically, panel (a) demonstrates these relative contributions in rigid CURATED COFs where, depending on the material, Coulombic interactions can be much stronger/weaker than vdW interactions (Coulombic/vdW interaction percentages mostly between ≈0.1–100%). Comparing charge-based interaction contributions, it can be understood that PACMOF charge-based interaction contributions tend to be larger than those that are DDEC6 and PACMAN charge-based despite having some exceptions. Note that these contributions are very similar in the case of DDEC6 and PACMAN charge-based cases. In general, there is not a clear trend between interaction contributions and PLD as evidenced by structures with PLDs around 30 Å where both very high and low Coulombic/vdW interaction percentages can be observed, depending on material. To investigate some of the cases where Coulombic interactions are small compared to vdW interactions (Coulombic/vdW interaction percentage < 5%), several structures are selected for further analysis. These selected structures with different PLDs are employed in NVT MD simulations from which snapshots are obtained which are subsequently used in GCMC simulations to estimate the effect of intrinsic flexibility on interaction contributions. Panel (b) shows

© 2025 The Author(s). Advanced Theory and Simulations published by Wiley-VCH GmbH

25130390, 0, Downloaded from https://advanced.onlinelibrary.wiley.com/doi/10.1002/adts.202500060 by Ozyegin University, Wiley Online Library on [04/09/2025]. See the Terms and Conditions (https://onlinelibrary.wiley.com/terms-and-conditions) on Wiley Online Library for rules of use; OA articles are governed by the applicable Creative Commons License

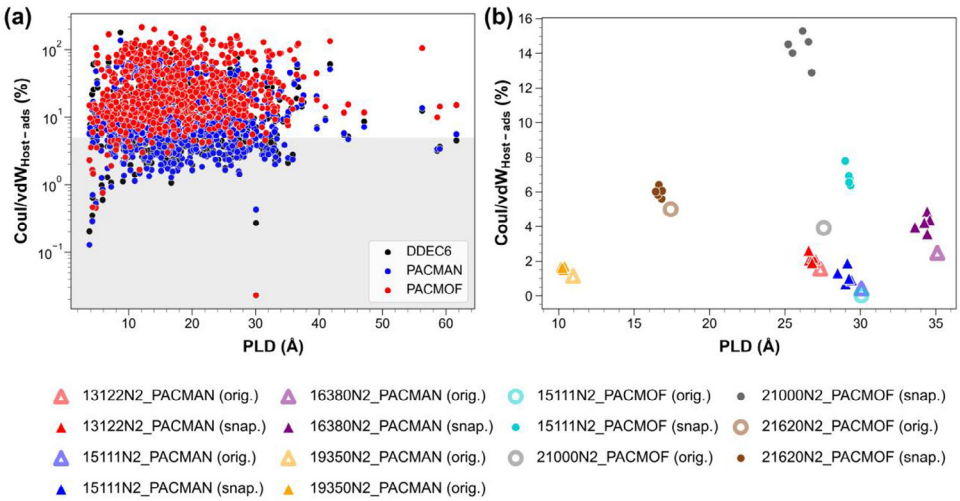

Figure 7. The percentage of Coulombic interactions over vdW interactions calculated at 1 bar, 298 K between host and adsorbates in a) rigid CURATED COFs, and b) rigid and MD snapshots of CURATED COFs. In panel (a), area under 5% is shaded in grey from which some structures are selected for panel (b).

the interaction contributions with respect to PLDs where results for rigid and MD snapshots of CURATED COFs are compared. Depending on the extent of intrinsic flexibility effects, Coulombic/vdW interaction percentages can differ by several folds as exemplified by CURATED COFs labelled as 15111N2 and 21000N2 with PACMOF charges (PLDs of ≈25–30 Å). On the other hand, the role of intrinsic flexibility effects on interaction contribution can remain limited for some structures with much different PLDs (e.g., 19350N2 and 13122N2 with PACMAN charges).

As the intrinsic flexibility of frameworks can affect the separation performance metrics as well, these metrics are investigated for MD snapshots of several CURATED COFs to compare with their rigid counterparts. Comparing these metrics in **Figure 8**, it can be concluded that the changes in metrics do not follow the same trend for all structures implying that ranking differences

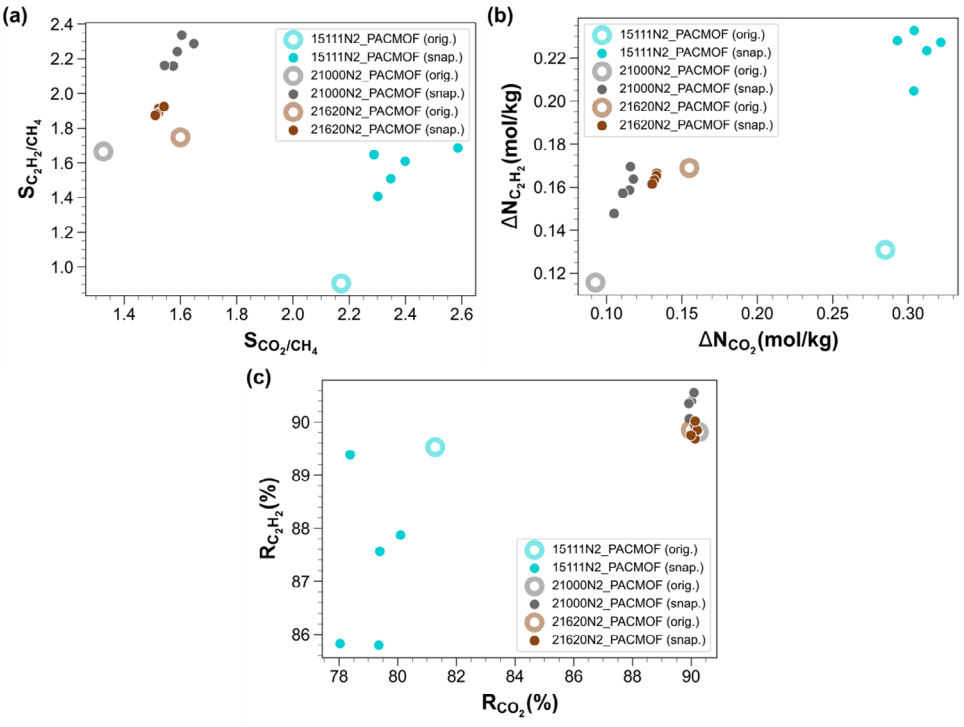

Figure 8. Comparison of separation performance metrics a) selectivity, b), working capacity, and c) regenerability) of rigid and MD snapshots of CURATED COFs.

© 2025 The Author(s). Advanced Theory and Simulations published by Wiley-VCH GmbH

25130390, 0, Downloaded from https://advanced.onlinelibrary.wiley.com/doi/10.1002/adts.202500060 by Ozyegin University, Wiley Online Library on [04/09/2025]. See the Terms and Conditions (https://onlinelibrary.wiley.com/terms-and-conditions) on Wiley Online Library for rules of use; OA articles are governed by the applicable Creative Commons License

could have been observed if flexibility effects had been taken into account.

To sum up, the effect of partial atomic charges on $C_2H_2/CO_2/CH_4$ separation performances is investigated using DDEC6, PACMAN, and PACMOF charges. DDEC6, and PACMAN charge-based results (i.e., separation performance metrics, atomic charges, isotherms, RDFs, interaction contributions) are found to be very similar. In general, PACMOF charge-based results show some drastic disparities compared to DDEC6 and PACMAN charges, especially in terms of adsorption isotherms, and separation performance metrics. It is hoped that this work will help improve the understanding of role of partial atomic charges in COFs regarding $C_2H_2/CO_2/CH_4$ separation and guide the future studies on the selection of charges used in COFs for GCMC simulations, in general.

4. Conclusion

In this work, the $C_2H_2/CO_2/CH_4$ (0.33/0.33/0.33) separation performances of ≈700 CURATED COFs at 298 K are studied using two ML models, PACMAN and PACMOF, to understand which ML model enables rapidly obtaining accurate separation performances as compared to reference DDEC6 method-based results. As a first step, the charge distributions per element type in all CURATED COFs are investigated where similar distributions of DDEC6 and PACMAN charges are observed. In comparison with DDEC6 and PACMAN charge distributions, PACMOF charge distributions involve considerable disparities especially for some specific elements such as Cu, Co, and P. To understand which charge prediction method (PACMAN or PACMOF) can better reproduce separation performances obtained using DDEC6 charges, distributions and ratios of separation performances are compared. It has been observed that, in general, separation performances and material rankings acquired using PACMAN charges are more similar with those calculated using DDEC6 charges. Specifically, the top 20 materials based on PACMOF charges are highly dissimilar to those based on DDEC6 or PACMAN charges. Examining six performance metrics of top 10 CURATED COFs, most of them excel at ΔN_{C2H2}, R_{C2H2}, and R_{CO2} while there are a few cases where selectivities are high despite having relatively low working capacity, and regenerability.

To better comprehend the disparities caused by different charges, the top CURATED COF (12011N2) based on PACMOF charges has been investigated. It has been found that C_2H_2, CO_2, and CH_4 adsorption isotherms differ significantly as DDEC6 and PACMAN charge-based isotherms are compared with PACMOF charge-based isotherms. This material also highlights the close agreement between PACMAN and DDEC6 charge-based results, as their isotherms and RDFs are nearly identical. Analysis of charge differences by element type in 12011N2 reveals that PACMAN charges more closely represent DDEC6 charges than PACMOF charges. Examining Coulombic/vdW interaction percentages, PACMOF charges generally result in higher values than those based on DDEC6 and PACMAN charges. Comparing these contributions in rigid and flexible MD snapshots of CURATED COFs, it can be concluded that flexibility effects can influence Coulombic/vdW interaction percentages to varying extents. Finally, when considering the contribution of each separation performance metric to the total separation performance score of COF materials, it has been observed that, for most of the top 10 materials, working capacity and regenerability contribute more than adsorption selectivity.

Supporting Information

Supporting Information is available from the Wiley Online Library or from the author.

Acknowledgements

The authors acknowledge TUBITAK 2218 Program funding. This publication was composed through the support of TUBITAK-2218-National Postdoctoral Research Fellowship Program (Project No: 122C227). However, the entire responsibility for the publication belongs to the publication authors. The financial support received from TUBITAK does not mean that the content of the publication is endorsed by TUBITAK scientifically. The numerical calculations reported in this paper were partially performed at TUBITAK ULAKBIM, High Performance and Grid Computing Center (TRUBA resources). Computing resources used in this work were partially provided by the National Center for High Performance Computing of Turkey (UHeM) under grant number 1009312021.

Conflict of Interest

The authors declare no conflict of interest.

Author Contributions

All simulations were performed by H.D. H.D. and I.E. contributed to the conceptualization, writing, data curation, and design of methodology employed in this study. I.E. supervised the study. All authors have given approval to the final version of the manuscript.

Data Availability Statement

The data that support the findings of this study are available from the corresponding author upon reasonable request.

Keywords

acetylene, adsorption, atomic charge, computational chemistry, covalent-organic framework

Received: January 10, 2025
Revised: May 8, 2025
Published online:

[1] H. Schobert, *Chem. Rev.* **2014**, *114*, 1743.
[2] R.-H. Su, W.-J. Shi, X.-Y. Zhang, L. Hou, Y.-Y. Wang, *Inorg. Chem.* **2023**, *62*, 11869.
[3] Y. Zhang, Y. Han, B. Luan, L. Wang, W. Yang, Y. Jiang, T. Ben, Y. He, B. Chen, *J. Am. Chem. Soc.* **2024**, *146*, 17220.
[4] M. L. Foo, R. Matsuda, Y. Hijikata, R. Krishna, H. Sato, S. Horike, A. Hori, J. Duan, Y. Sato, Y. Kubota, M. Takata, S. Kitagawa, *J. Am. Chem. Soc.* **2016**, *138*, 3022.

© 2025 The Author(s). Advanced Theory and Simulations published by Wiley-VCH GmbH

25130390, 0, Downloaded from https://advanced.onlinelibrary.wiley.com/doi/10.1002/adts.202500060 by Ozyegin University, Wiley Online Library on [04/09/2025]. See the Terms and Conditions (https://onlinelibrary.wiley.com/terms-and-conditions) on Wiley Online Library for rules of use; OA articles are governed by the applicable Creative Commons License

[5] N. Huang, P. Wang, D. Jiang, *Nat. Rev. Mater.* **2016**, *1*, 16068.
[6] Z. Wang, S. Zhang, Y. Chen, Z. Zhang, S. Ma, *Chem. Soc. Rev.* **2020**, *49*, 708.
[7] P. J. Waller, F. Gándara, O. M. Yaghi, *Acc. Chem. Res.* **2015**, *48*, 3053.
[8] R. Liu, K. T. Tan, Y. Gong, Y. Chen, Z. Li, S. Xie, T. He, Z. Lu, H. Yang, D. Jiang, *Chem. Soc. Rev.* **2021**, *50*, 120.
[9] D. Ongari, A. V Yakutovich, L. Talirz, B. Smit, *ACS Cent. Sci.* **2019**, *5*, 1663.
[10] Z. Wang, Y. Zhang, T. Wang, E. Lin, T. Wang, Y. Chen, P. Cheng, Z. Zhang, *Small* **2023**, *19*, 2303684.
[11] A. L. Myers, J. M. Prausnitz, *AIChE J.* **1965**, *11*, 121.
[12] Y. Wang, J. Xie, Z. Ren, Z.-H. Guan, *Chem. Eng. J.* **2022**, *448*, 137687.
[13] L. Chen, C. Gong, X. Wang, F. Dai, M. Huang, X. Wu, C.-Z. Lu, Y. Peng, *J. Am. Chem. Soc.* **2021**, *143*, 10243.
[14] W. Jiang, P. Wang, K. Otake, S. Kitagawa, Y. Noda, K. Takeda, K. Takegoshi, *J. Phys. Chem. C* **2022**, *126*, 15367.
[15] S. Liu, C. Hao, C. Meng, S. Liu, W. Zhai, Q. Zhu, W. Li, S. Wei, Z. Wang, X. Lu, *ACS Appl. Nano Mater.* **2023**, *6*, 12124.
[16] G. Wang, Z. Wang, W. Cao, Y. Liu, B. Zheng, Y. Deng, *Comput. Theor. Chem.* **2022**, *1210*, 113655.
[17] G. O. Aksu, S. Keskin, *ACS Appl. Mater. Interfaces* **2024**, *16*, 19806.
[18] J. S. De Vos, S. Ravichandran, S. Borgmans, L. Vanduyfhuys, P. Van Der Voort, S. M. J. Rogge, V. Van Speybroeck, *Chem. Mater.* **2024**, *36*, 4315.
[19] J. Ning, K. Shen, R. Zhao, K. Gao, J. Cai, L. Hou, *J. Phys. Chem. C* **2024**, *128*, 11355.
[20] S. Yang, W. Zhu, L. Zhu, X. Ma, T. Yan, N. Gu, Y. Lan, Y. Huang, M. Yuan, M. Tong, *ACS Appl. Mater. Interfaces* **2022**, *14*, 56353.
[21] C. Altintas, S. Keskin, *Mol. Syst. Des. Eng.* **2020**, *5*, 532.
[22] R. Wang, Y. Zhong, L. Bi, M. Yang, D. Xu, *ACS Appl. Mater. Interfaces* **2020**, *12*, 52797.
[23] C. E. Wilmer, M. Leaf, C. Y. Lee, O. K. Farha, B. G. Hauser, J. T. Hupp, R. Q. Snurr, *Nat. Chem.* **2012**, *4*, 83.
[24] C. Zou, D. R. Penley, E. H. Cho, L.-C. Lin, *J. Phys. Chem. C* **2020**, *124*, 11428.
[25] J. Burner, J. Luo, A. White, A. Mirmiran, O. Kwon, P. G. Boyd, S. Maley, M. Gibaldi, S. Simrod, V. Ogden, T. K. Woo, *Chem. Mater.* **2023**, *35*, 900.
[26] J. Luo, O. Ben Said, P. Xie, M. Gibaldi, J. Burner, C. Pereira, T. K. Woo, *npj Comput. Mater.* **2024**, *10*, 224.
[27] F. L. Oliveira, C. Cleeton, R. Neumann Barros Ferreira, B. Luan, A. H. Farmahini, L. Sarkisov, M. Steiner, *Sci. Data* **2023**, *10*, 230.
[28] D. Ongari, P. G. Boyd, O. Kadioglu, A. K. Mace, S. Keskin, B. Smit, *J. Chem. Theory Comput.* **2019**, *15*, 382.
[29] S. Kancharlapalli, A. Gopalan, M. Haranczyk, R. Q. Snurr, *J. Chem. Theory Comput.* **2021**, *17*, 3052.
[30] L. Wei, R. Zizhen, C. Y. G., L. Song, *ChemistrySelect* **2017**, *2*, 9458.
[31] A. K. Rappe, W. A. Goddard, *J. Phys. Chem.* **1991**, *95*, 3358.
[32] T. A. Manz, D. S. Sholl, *J. Chem. Theory Comput.* **2010**, *6*, 2455.
[33] T. A. Manz, D. S. Sholl, *J. Chem. Theory Comput.* **2012**, *8*, 2844.
[34] C. E. Wilmer, K. C. Kim, R. Q. Snurr, *J. Phys. Chem. Lett.* **2012**, *3*, 2506.
[35] E. S. Kadantsev, P. G. Boyd, T. D. Daff, T. K. Woo, *J. Phys. Chem. Lett.* **2013**, *4*, 3056.
[36] C. Campañá, B. Mussard, T. K. Woo, *J. Chem. Theory Comput.* **2009**, *5*, 2866.
[37] V. V Korolev, A. Mitrofanov, E. I. Marchenko, N. N. Eremin, V. Tkachenko, S. N. Kalmykov, *Chem. Mater.* **2020**, *32*, 7822.
[38] T. D. Pham, F. Joodaki, F. Formalik, R. Q. Snurr, *J. Phys. Chem. C* **2024**, *128*, 17165.
[39] G. O. Aksu, S. Keskin, *ACS Mater. Lett.* **2025**, *7*, 954.
[40] Y. Lang, L. Sun, Y. Pan, M. Xu, D. Zhai, J. Liu, W. Deng, L. Yang, *Chem. Eng. Sci.* **2025**, *305*, 121175.
[41] Y. Qiu, L. Chen, X. Zhang, D. Ping, Y. Tian, Z. Zhou, *AIChE J.* **2024**, *70*, 18575.
[42] G. Zhao, Y. G. Chung, *J. Chem. Theory Comput.* **2024**, *20*, 5368.
[43] Y. G. Chung, E. Haldoupis, B. J. Bucior, M. Haranczyk, S. Lee, H. Zhang, K. D. Vogiatzis, M. Milisavljevic, S. Ling, J. S. Camp, B. Slater, J. I. Siepmann, D. S. Sholl, R. Q. Snurr, *J. Chem. Eng. Data* **2019**, *64*, 5985.
[44] A. S. Rosen, S. M. Iyer, D. Ray, Z. Yao, A. Aspuru-Guzik, L. Gagliardi, J. M. Notestein, R. Q. Snurr, *Matter* **2021**, *4*, 1578.
[45] K. M. Jablonka, D. Ongari, S. M. Moosavi, B. Smit, *Chem. Rev.* **2020**, *120*, 8066.
[46] T. A. Manz, N. G. Limas, *RSC Adv.* **2016**, *6*, 47771.
[47] N. G. Limas, T. A. Manz, *RSC Adv.* **2016**, *6*, 45727.
[48] T. A. Manz, *RSC Adv.* **2017**, *7*, 45552.
[49] N. G. Limas, T. A. Manz, *RSC Adv.* **2018**, *8*, 2678.
[50] A. V Marenich, S. V Jerome, C. J. Cramer, D. G. Truhlar, *J. Chem. Theory Comput.* **2012**, *8*, 527.
[51] R. F. W. Bader, P. J. MacDougall, C. D. H. Lau, *J. Am. Chem. Soc.* **1984**, *106*, 1594.
[52] R. F. W. Bader, C. F. Matta, *J. Phys. Chem. A* **2004**, *108*, 8385.
[53] D. Dubbeldam, S. Calero, D. E. Ellis, R. Q. Snurr, *Mol. Simul.* **2016**, *42*, 81.
[54] M. Fischer, F. Hoffmann, M. Fröba, *ChemPhysChem* **2010**, *11*, 2220.
[55] W. L. Jorgensen, J. D. Madura, C. J. Swenson, *J. Am. Chem. Soc.* **1984**, *106*, 6638.
[56] J. J. Potoff, J. I. Siepmann, *AIChE J.* **2001**, *47*, 1676.
[57] M. G. Martin, J. I. Siepmann, *J. Phys. Chem. B* **1998**, *102*, 2569.
[58] S. L. Mayo, B. D. Olafson, W. A. Goddard, *J. Phys. Chem.* **1990**, *94*, 8897.
[59] A. K. Rappe, C. J. Casewit, K. S. Colwell, W. A. Goddard, W. M. Skiff, *J. Am. Chem. Soc.* **1992**, *114*, 10024.
[60] P. P. Ewald, *Ann. Phys.* **1921**, *64*, 253.
[61] T. F. Willems, C. H. Rycroft, M. Kazi, J. C. Meza, M. Haranczyk, *Microporous Mesoporous Mater.* **2012**, *149*, 134.
[62] D. Ongari, P. G. Boyd, S. Barthel, M. Witman, M. Haranczyk, B. Smit, *Langmuir* **2017**, *33*, 14529.
[63] D. Fairen-Jimenez, S. A. Moggach, M. T. Wharmby, P. A. Wright, S. Parsons, T. Düren, *J. Am. Chem. Soc.* **2011**, *133*, 8900.
[64] X.-C. Huang, Y.-Y. Lin, J.-P. Zhang, X.-M. Chen, *Angew. Chem., Int. Ed.* **2006**, *45*, 1557.
[65] J. A. Gee, D. S. Sholl, *J. Phys. Chem. C* **2016**, *120*, 370.
[66] S. Plimpton, *J. Comput. Phys.* **1995**, *117*, 1.
[67] A. P. Thompson, H. M. Aktulga, R. Berger, D. S. Bolintineanu, W. M. Brown, P. S. Crozier, P. J. in 't Veld, A. Kohlmeyer, S. G. Moore, T. D. Nguyen, R. Shan, M. J. Stevens, J. Tranchida, C. Trott, S. J. Plimpton, *Comput. Phys. Commun.* **2022**, *271*, 108171.
[68] D. Frenkel, B. Smit, *Understanding Molecular Simulation: From Algorithms to Applications*, Academic Press, San Diego, CA **2002**.
[69] P. G. Boyd, S. M. Moosavi, M. Witman, B. Smit, *J. Phys. Chem. Lett.* **2017**, *8*, 357.
[70] M. Agrawal, D. S. Sholl, *ACS Appl. Mater. Interfaces* **2019**, *11*, 31060.

© 2025 The Author(s). Advanced Theory and Simulations published by Wiley-VCH GmbH

25130390, 0, Downloaded from https://advanced.onlinelibrary.wiley.com/doi/10.1002/adts.202500060 by Ozyegin University, Wiley Online Library on [04/09/2025]. See the Terms and Conditions (https://onlinelibrary.wiley.com/terms-and-conditions) on Wiley Online Library for rules of use; OA articles are governed by the applicable Creative Commons License